

Satellite Holmium M -Edge Spectra from the Magnetic Phase via Resonant Soft X-Ray Scattering

Tatsuya NAGAO^{1*} and Jun-ichi IGARASHI²

¹*Faculty of Engineering, Gunma University, Kiryu, Gunma 376-8515, Japan*

²*Faculty of Science, Ibaraki University, Mito, Ibaraki 310-8512, Japan*

Developing an expression of resonant x-ray scattering (RXS) amplitude which is convenient for investigating the contributions from the higher rank tensor on the basis of a localized electron picture, we analyze the RXS spectra from the magnetic phases of Ho near the $M_{4,5}$ absorption edges. At the M_5 edge in the uniform helical phase, the calculated spectra of the absorption coefficient, the RXS intensities at the first and second satellite spots capture the properties the experimental data possess, such as the spectral shapes and the peak positions. This demonstrates the plausibility of the adoption of the localized picture in this material and the effectiveness of the spectral shape analysis. The latter point is markedly valuable since the azimuthal angle dependence, which is one of the most useful informations RXS can provides, is lacking in the experimental conditions. Then, by focusing on the temperature dependence of the spectral shape at the second satellite spot, we expect that the spectrum is the contribution of the pure rank two profile in the uniform helical and the conical phases while that is dominated by the rank one profile in the intermediate temperature phase, so-called spin slip phase. The change of the spectral shape as a function of temperature indicates a direct evidence of the change of magnetic structures undergoing. Furthermore, we predict that the intensity, which is the same order observed at the second satellite spot, is expected at the fourth satellite spot from the conical phase in the electric dipolar transition.

KEYWORDS: resonant x-ray scattering, Ho metal, amplitude formula, satellite spot signal, helical magnetic structure

1. Introduction

With the advent of the so-called third generation synchrotron sources, resonant x-ray scattering (RXS) has opened a new research field of investigating, for example, the multipole ordering phases in the f electron systems due to the electric multipolar transitions. RXS is a second order optical process that an incident photon with the energy tuned through an absorption edge excites the core electron to an unoccupied level, then the excited electron decays into the core level accompanied by emission of a photon. Element, electron shell, and chemical valence specific natures of the RXS technique have made it possible to become a complement to neutron scattering to elucidate the spatial Fourier transform of the multipole order such as quadrupole and octupole as well as dipole moments.^{24–26, 28, 29, 31, 33}

*E-mail:tnagao@phys.sci.gunma-u.ac.jp

Historically, however, analysis of the magnetic properties on the magnetic materials in terms of the x-ray resonant process, so-called resonant magnetic x-ray scattering (RMXS), developed in its own right since Blume suggested a possibility of such a usage.⁵ The first observation of RMXS was made by Namikawa *et al.* on ferromagnetic nickel.⁸ Since then, further studies followed, investigating, in particular, the f electron systems such as holmium, uranium arsenide, and so on.^{10,12,14}

Metallic holmium is one of the most studied materials by using RMXS. The crystal structure of holmium is hexagonal close packed structure with lattice constants $a = 3.58$ Å and $c = 5.62$ Å at room temperature. On cooling down the temperature, magnetic moments in Ho order at $T_N = 133$ K with a helical magnetic structure, which consists of the ferromagnetically aligned moments within each basal plane and the orientation of the moments rotates in successive basal planes. As the temperature decreases, the wavevector characterizing the spatial modulation of the helical pattern reduces and locks in below $T_C = 20$ K where the magnetic structure becomes a conical configuration.^{1,2}

Gibbs *et al.* detected the RMXS signals near the Ho L_3 edge in the magnetic satellite spots.¹⁰ Polarization analysis distinguished two kinds of spectra with peak positions separated about 6 eV. They are attributed to the consequences of the electric dipole ($E1$) and quadrupole ($E2$) transitions. The former had intensities up to the second harmonic satellite spot while the latter was up to the fourth harmonic satellite spot. Hannon *et al.* gave the theoretical explanation of the experimental results.¹¹ They derived useful formulae describing the RMXS amplitude and, by using them, concluded that relatively large scattering amplitude would be expected in the vicinity of the Ho $L_{2,3}$ and $M_{4,5}$ edges, the former of which explained the experiment. By extending the formula derived by Hannon *et al.*, Hill and McMorow investigated some qualitative properties of the RXS signals at the Ho L_3 edge in the uniform helimagnetic and the conical phases.²³ These works have stimulated the immense activities in the field of RMXS both experimentally and theoretically.³⁰

As for Ho, several experiments followed focusing, for instance, on the temperature dependence of the exponents, the existence of two-length scales, and so on.^{13,16,17} Theoretical analyses based on the mean field model revealed the importance of the interaction having the trigonal symmetry.^{20,22} Despite the numerous achievements provided by the RMXS data at the Ho L_3 edge, it is difficult to extract the quantitative interpretation since the $E1$ process at the L_3 edge is the consequence of the transition between the $2p$ and $5d$ states so that the relevancy of the $4f$ electrons is indirect. The band nature of the $5d$ electrons also increases the complication of the analysis. Although the $E2$ signal, the transition between the $2p$ and $4f$ states, presents a direct information of the $4f$ electrons, the interference with the $E1$ signal complicates the quantitative interpretation.

A possibility has long been suggested that the RMXS measurement at the Ho $M_{4,5}$ edges

by means of soft x-ray beam may supply the useful insights to elucidate the natures of the magnetic structures.¹¹ The $E1$ processes at the $M_{4,5}$ edges are brought about by the transition between the $3d$ and $4f$ states, which provides a direct information from the $4f$ electrons. Furthermore, long wavelength of the soft x-ray is suitable for investigating the long period magnetic structure of Ho. Recently, Spencer *et al.* and Ott *et al.* have succeeded in detecting the RMXS spectra of the first and second harmonics satellite spots as well as the absorption coefficient spectrum at the Ho M_5 edge from the helical magnetic phase.^{34,38} The energy profiles of the spectra of the first and second satellite spots differ significantly from each other. They were attributed to the circular and linear dichroic contributions, respectively. In this case, it turned out that the absence of the $E2$ contribution made the analysis rather simple. These facts make a sharp contrast observed at the L_3 edge where the difference of the spectral shapes at the different satellite spots were not so prominent.¹⁰

Usually, the azimuthal angle (ψ) dependence of the peak intensity of the spectrum offers one of the most highlighted outcomes given by the R(M)XS experiment in many cases. In holmium, however, the intensity shows no ψ dependence in the uniform helical and conical phases with the choice of the scattering vector adopted in the experiment. Therefore, we should extract implications as many as possible through the spectral analysis. Then, a theoretical study may lend support to the analysis of the R(M)XS spectra at the $M_{4,5}$ edges.

In this paper, therefore, we perform a theoretical spectral analysis of RMXS at the Ho $M_{4,5}$ edge. Based on a localized electron picture, we calculate the spectra exploiting a useful expression of the scattering amplitude whose utility is examined in several f electron systems.^{35–37} We investigate three spectra; the RMXS spectra at the first and second satellite spots and the absorption spectrum. Their shapes at the M_5 edge are distinguishable one another and capture the main features presented by the experiment, spectral shape and the shift of the peak position at the different rank satellite spots. The ratio of the peak intensity extracted from the calculated spectra also is the same order as the experimental one.

Another result we present is a prediction that the spectral shape varies as a function of temperature. For instance, the spectrum at the second satellite spot shows the same energy profiles both in the helical and conical phases. On the other hand, the profile becomes completely different one in the temperature range between two phases, known so-called as the spin slip phase. Such an evolution of the spectral shape may provide the direct evidence that the change of the magnetic structure is undergoing.

Further inferred from our investigation is a possibility of the observation of the RXS spectra at the higher-order satellite spots. In the conical phase, the presence of fifth- and seventh-order magnetic satellites in the neutron scattering were observed.¹ This is attributed to the fact that the turn angle of the magnetic moment between successive Ho planes is not a constant (see Fig. 1 (b)). Similarly, we show that the RXS intensities are expected at the

higher-order satellite spots in this phase. For example, in the $E1$ transition, fourth-, fifth-, seventh-, and eighth-order satellites are possible to be detected. Our estimation reveals that the RXS spectrum at the Ho M_5 fourth-order satellite spot from the $\pi - \sigma'$ channel possesses the same order of magnitude and the same energy profile as that observed by Ott *et al.* at the second satellite spot.

The $E1$ transition at $M_{4,5}$ edges of rare earth metals give rise to an excitation of electron from the $3d$ levels to the $4f$ levels. Since the associated photon energy is about $1 \sim 2$ KeV, this process is only useful to investigate the long-range orders with rather long periods in comparison with the lattice constant. In this paper, taking up the helical and conical magnetic orders in Ho metal, we analyze the RXS spectra in detail

The organization of this manuscript is as follows. In Sect. 2, we explain the various magnetic structures exhibited by Ho. In Sec. 3, we present a brief summary of the theoretical framework of R(M)XS. An expression of the R(M)XS amplitude the present authors had derived^{35,37} is introduced and is compared with the previous similar results.^{11,18,19,21,23,27} In Sec. 4, the initial and the intermediate states needed to calculate the RXS spectra are defined in order to apply the theory to the investigation of the RMXS spectra of the satellite spots in the vicinity of the Ho M_5 edge. Qualitative features expected from each phases are analyzed in Sec. 5. Numerically calculated spectra of the absorption coefficient and RMXS are shown and compared with the experiment in Sec. 6. Main conclusions are summarized in Sect. 7.

2. Magnetic ordering phases of Ho metal

Before calculating the RXS spectra, we summarize the magnetic structures experimentally identified in the Ho metal. The crystal takes an hcp structure. Below $T_N = 133$ K, the magnetic moments of the system order in a helical structure. The moments on each Ho layer are confined to the basal plane and are coupled ferromagnetically within each layer. The interlayer angle of the moment varies a constant angle per layer. We call it as "*uniform helical phase*". A schematic explanation of the orientation of the moment on each layer of this phase is given in Fig. 1 (a). The number of Ho layers N within one helical pitch is connected to the modulation vector $\mathbf{q} = (0, 0, 2/N)$ in units of $2\pi/c$. The N increases on cooling because the helical structure is distorted, or more precisely, the magnitude of \mathbf{q} reduces from $\mathbf{q} = (0, 0, 0.271)$ corresponding to $N \simeq 7$ just below T_N to $\mathbf{q} = (0, 0, \frac{1}{6})$ corresponding to $N = 12$ at $T_C = 20$ K. Below $T_{textrm{C}}$, \mathbf{q} is locked in to $(0, 0, \frac{1}{6})$ corresponding to $N = 12$ with the emergence of a ferromagnetic component along the c -axis, called as "*conical phase*". A complication is that the orientation of the moment within a basal plane does not alters constantly.^{3,9}

The magnetic easy axes seem to direct to the centers of six triangles formed by neighboring atoms. The actual structure in the conical phase is that the twelve Ho layers form six pairs of two layers with the moments directing nearly to one of the centers of six triangles formed by nearest neighbor atoms as shown in Fig. 1 (b). The bunching angle between the pairs across

the same easy axis is defined as γ and evaluated about 5.8° in the $T \rightarrow 0$ limit.

The transition between the uniform helical and the conical phases is not a straightforward depending on the conditions such as the strain present in the sample, the presence of the chemical impurities, and so on.¹⁷ When the temperature is above T_C but well below T_N , the c component of the moment disappears but the bunching remains. At the same time, some of the pairs lose their partner and the remaining moment directs to one of the centers of six triangles formed by nearest neighbor atoms. Gibbs *et al.* called this phase as the "spin slip phase". For example, when one pair experiences a spin slip, the unit cell of the system becomes five bunched pairs plus a single component with $N = 11$ (See Fig. 1 (c)). When the temperature raises, the value of γ increases resulting in the uniform helical phase. In this paper, we show that the spectral shapes of the RXS spectra changes drastically when the magnetic structure changes from the uniform helical one to the others.

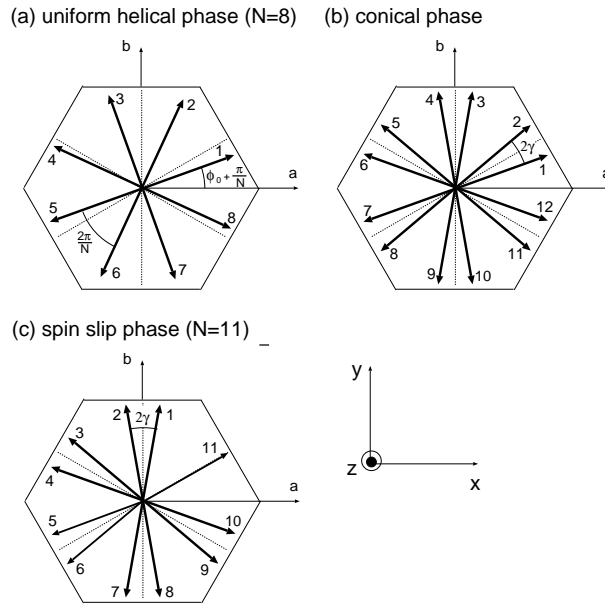


Fig. 1. Orientation of the magnetic moment projected onto the ab plane: (a) uniform helical phase with $N = 8$, (b) conical phase, and (c) spin slip phase with $N = 11$. Direction of arrow associated with number $n = 1, \dots, N$ represents the direction of the magnetic moment in the n -th Ho layer. The dotted lines denote six equivalent easy axes.

3. An extension of the RXS formula of Hannon *et al.*

A resonant process is described as following: an incident photon with the energy $\hbar\omega$, wave vector \mathbf{k} , and polarization ϵ is scattered into the state with the energy $\hbar\omega'$, wave vector \mathbf{k}' , and polarization ϵ' through the process that the core electron is excited into an unoccupied level leaving a core hole and then recombines with the core hole by emitting the photon.

In a localized electron picture, the scattering amplitude is well approximated by a sum of the contributions from each site. Therefore, the RXS amplitude $f_{E1}(\boldsymbol{\epsilon}, \boldsymbol{\epsilon}', \mathbf{k}, \mathbf{k}'; \omega)$ in the $E1$ transition is given by

$$f_{E1} = \frac{1}{\sqrt{N_0}} \sum_j e^{-i\mathbf{G} \cdot \mathbf{r}_j} M_j(\boldsymbol{\epsilon}, \boldsymbol{\epsilon}'; \omega), \quad (3.1)$$

with

$$M_j(\boldsymbol{\epsilon}, \boldsymbol{\epsilon}'; \omega) = \sum_{\alpha' \alpha} \epsilon'_{\alpha'} \epsilon_{\alpha} \sum_{\Lambda} \frac{\langle 0_j | x_{\alpha, j} | \Lambda \rangle \langle \Lambda | x_{\alpha', j} | 0_j \rangle}{\hbar\omega - (E_{\Lambda} - E_0) + i\Gamma}, \quad (3.2)$$

within the second order of the photon-electron interaction in the perturbation theory. Here the scattering vector is defined as $\mathbf{G} = \mathbf{k}' - \mathbf{k}$, and the number of sites is represented as N_0 . The $M_j(\boldsymbol{\epsilon}, \boldsymbol{\epsilon}'; \omega)$ is the scattering amplitude of single site j with the position vector \mathbf{r}_j , where the initial state is represented as $|0_j\rangle$ with the energy E_0 and the intermediate state is given by $|\Lambda\rangle$ with the energy E_{Λ} . The lifetime broadening width of the core hole is denoted as Γ . The dipole operators $x_{\alpha}(j)$'s are defined as $x_1(j) = x$, $x_2(j) = y$, and $x_3(j) = z$ in the coordinate system fixed to the crystal axes with the origin located at the site j . The RXS intensity is proportional to the square of the absolute value of the scattering amplitude.

The evaluation of eq. (3.2) is not an easy task, because the intermediate states are to be summed up. We consider the situation that the initial state is described within a multiplet of certain total angular momentum J , and the degeneracy is lifted by the crystal electric field (CEF) and the inter-atomic interaction. This situation is familiar in many f electron systems. On the other hand, we neglect the CEF and the inter-atomic interaction on the intermediate states. This may be justified because the energy dependence of the spectra is mainly determined by the multiplets which energy is much larger than the CEF and the inter-atomic interaction. With assumption, the intermediate states possess the rotational symmetry, and thereby the summation over these states are rather simply carried out. We could express the scattering amplitude at site j in a simple form as

$$\begin{aligned} M_j &= \alpha_{E1}^{(0)}(\omega)(\boldsymbol{\epsilon}' \cdot \boldsymbol{\epsilon}) - i\alpha_{E1}^{(1)}(\omega)(\boldsymbol{\epsilon}' \times \boldsymbol{\epsilon}) \cdot \langle 0_j | \hat{\mathbf{J}} | 0_j \rangle \\ &+ \alpha_{E1}^{(2)}(\omega) \sum_{\nu=1}^5 P_{\nu}^{(2)}(\boldsymbol{\epsilon}, \boldsymbol{\epsilon}') \langle 0_j | \hat{z}_{\nu} | 0_j \rangle. \end{aligned} \quad (3.3)$$

Here $\alpha_{E1}^{(n)}(\omega)$ represents the energy profile of rank n operator, which depends only on the initial state through the magnitude of the angular momentum J . The geometrical factors associated with the rank two quantities are represented as $P_{\nu}^{(2)}(\boldsymbol{\epsilon}, \boldsymbol{\epsilon}')$. The components of the (rank two)

quadrupole operator are defined as

$$\hat{z}_\nu = \begin{cases} \hat{O}_{x^2-y^2} = \frac{\sqrt{3}}{2}(\hat{J}_x^2 - \hat{J}_y^2), & \nu = 1 \\ \hat{O}_{3z^2-r^2} = \frac{1}{2}[3\hat{J}_z^2 - J(J+1)], & \nu = 2 \\ \hat{O}_{yz} = \frac{\sqrt{3}}{2}(\hat{J}_y\hat{J}_z + \hat{J}_z\hat{J}_y), & \nu = 3 \\ \hat{O}_{zx} = \frac{\sqrt{3}}{2}(\hat{J}_z\hat{J}_x + \hat{J}_x\hat{J}_z), & \nu = 4 \\ \hat{O}_{xy} = \frac{\sqrt{3}}{2}(\hat{J}_x\hat{J}_y + \hat{J}_y\hat{J}_x), & \nu = 5 \end{cases}. \quad (3.4)$$

The detailed derivation of the above expression including the definitions of quantities $\alpha_{\text{E1}}^{(n)}(\omega)$ and $P_\nu^{(2)}(\epsilon, \epsilon')$ are found in our previous papers,³⁵⁻³⁷ in which applications to several f electron systems and an extension to the $E2$ process are explored too.

The formulae similar to eq. (3.3) are found in the previous literatures.^{11, 18, 21, 23} One of the most notable formulae is the one derived by Hannon *et al.*,¹¹ which is expressed for the magnetic ordered system as

$$M_j = (\epsilon' \cdot \epsilon) f'_0(\omega) - i(\epsilon' \times \epsilon) \cdot \mathbf{m}_j f'_1(\omega) + (\epsilon' \cdot \mathbf{m}_j)(\epsilon \cdot \mathbf{m}_j) f'_2(\omega), \quad (3.5)$$

where \mathbf{m}_j is the unit vector in the direction of the magnetic moment at site j . The energy profiles are represented by $f'_n(\omega)$'s describing the contributions from the order n of the magnetic moment. Although both are similar in a symmetrical point of view, our expression is more accurate and superior than that of Hannon *et al.* in the following reason.

First, higher rank multipole is naturally treated by our expression, while that of Hannon *et al.* was expressed in terms of the expectation values of the dipole moment operator. To make the comparison easy, we rewrite the last term of eq. (3.3) as

$$\begin{aligned} \alpha_{\text{E1}}^{(2)}(\omega) \sum_{\nu=1}^5 P_\nu^{(2)}(\epsilon, \epsilon') \langle 0_j | \hat{z}_\nu | 0_j \rangle \\ = \alpha_{\text{E1}}^{(2)}(\omega) \frac{3}{2} \left[\frac{1}{2} \langle (\epsilon \cdot \mathbf{J})(\epsilon' \cdot \mathbf{J}) + (\epsilon' \cdot \mathbf{J})(\epsilon \cdot \mathbf{J}) \rangle - \frac{J(J+1)}{3} (\epsilon' \cdot \epsilon) \right]. \end{aligned} \quad (3.6)$$

In comparison with Hannon *et al.*'s, the expectation value of the product of the operators is generally different from the product of the expectation values of the operators. Our expression is applicable to other multipole ordered phases without the local magnetic moment. The numerical amount of the difference between eqs. (3.3) and (3.5) depends on the system considered in the magnetic ordered phase. In the present case of holmium, the difference is relevant to the analysis of the second harmonics satellite spot, which brings about a quantitative outcome when we use eqs. (3.3) and (3.5) as a fitting function.

Second, our expression gives the spectral shape of the RXS intensity as a function of the incident photon energy, without relying on the so-called *fast collision* (FC) approximation. Recent development of the high resolution in energy enables the detection of the reliable spectral profiles as a function of the incident photon energy, which increases the value of our treatment including the energy dependence.

4. Procedure to evaluate the RXS amplitude in Ho

Before going to the detailed analysis of RXS spectra in Ho, we briefly explain how to evaluate eq. (3.3) based on a localized electron picture.

4.1 Evaluation of $\langle 0_j | \mathbf{J} | 0_j \rangle$ and $\langle 0_j | z_\nu | 0_j \rangle$

The holmium in the solid behaves, to a good approximation, as trivalent ion with the $(4f)^{10}$ configuration equivalent to \underline{f}^4 in the hole picture. We expect from Hund's rule the states of $^5\text{I}_8$ as the ground multiplet, which is denoted as $|J = 8, J_z\rangle$. The degeneracy of this multiplet would be lifted by the intersite interaction, resulting in the magnetically ordered states. Therefore, the magnetic wavefunctions at each site are expanded in terms of $|J = 8, J_z\rangle$'s. It is known that the local magnetic moment is as large as about $10\mu_B$ in the conical phase. This value is equivalent to the maximum one expected from the saturation value of $^5\text{I}_8$. It is also known that the local magnetic moment is about 70 % of the saturated value around $T/T_N \sim 0.6$ in the uniform helical phase. Accordingly, we assume that the magnetic moment at each Ho site is saturated, since the spectral shape of the energy profile $\alpha_{\text{E1}}^{(n)}(\omega)$ is not sensitive to the value. Therefore, the wavefunction is given by $|J = 8, J_z = 8\rangle$ at each site in the local coordinate frame where the z -axis is pointing to the direction of the local magnetic moment.

Let $(\theta_n, \beta, 0)$ be the Euler angle connecting the local coordinate frame to the crystal fixed frame for the n -th Ho layer, and $|\theta_n\rangle$ be the corresponding magnetic state. Then, the expectation values of the dipole and the quadrupole operators defined by the crystal fixed frame are evaluated as

$$\langle \theta_n | \begin{Bmatrix} \hat{J}_x \\ \hat{J}_y \\ \hat{J}_z \end{Bmatrix} | \theta_n \rangle = J \begin{Bmatrix} \sin \beta \cos \theta_n \\ \sin \beta \sin \theta_n \\ \cos \beta \end{Bmatrix}, \quad (4.1)$$

and

$$\langle \theta_n | \begin{Bmatrix} \hat{O}_2^2 \\ \hat{O}_2^0 \\ \hat{O}_{yz} \\ \hat{O}_{zx} \\ \hat{O}_{xy} \end{Bmatrix} | \theta_n \rangle = \frac{\sqrt{3}}{4} J(2J-1) \begin{Bmatrix} \sin^2 \beta \cos(2\theta_n) \\ \frac{1}{\sqrt{3}}(3\cos^2 \beta - 1) \\ \sin(2\beta) \sin \theta_n \\ \sin(2\beta) \cos \theta_n \\ \sin^2 \beta \sin(2\theta_n) \end{Bmatrix}. \quad (4.2)$$

These expressions are used for $\langle 0_j | \mathbf{J} | 0_j \rangle$ and $\langle 0_j | z_\nu | 0_j \rangle$ in eq. (3.3).

4.2 Evaluation of $\alpha_{\text{E1}}^{(i)}(\omega)$

Energy profiles $\alpha_{\text{E1}}^{(i)}(\omega)$ ($i = 0, 1, 2$) depend on the initial state only through J of the ground multiplet but little on the details of the magnetic orders. They also depend on the intermediate states. For the ground multiplet, we consider the intra-atomic Coulomb and the spin orbit (SO) interactions, where the parameters needed to evaluate the above interactions such as the Slater integrals for the Coulomb interaction and the SO coupling constant are

calculated within the Hartree-Fock (HF) approximation.^{?,40} Representing the Hamiltonian with the bases spanned by the \underline{f}^4 configuration, we diagonalize the Hamiltonian matrix. We obtain the degenerated lowest seventeen states corresponding to $J = 8$. In the intermediate states, the electronic configuration becomes $(3d)^9(4f)^{11}$ equivalent to $\underline{d}^1\underline{f}^3$. We repeat the similar procedure as have done to prepare the ground multiplet. The Hamiltonian describing the intermediate states takes full account of the intra-atomic Coulomb and the SO interactions among the $(3d)^9(4f)^{11}$ configuration. By diagonalizing numerically the Hamiltonian matrix represented with the bases spanned by the $\underline{d}^1\underline{f}^3$ configuration. We obtain the set of the intermediate states. These states are sufficient to evaluate the energy profiles $\alpha_{E1}^{(i)}(\omega)$.

5. Analysis of RXS for Ho

Since all the Ho atoms within the same layer give a same amount of contribution, the summation over site j is replaced by that over n . The amplitude for the m -th satellite spot is given by

$$\begin{aligned}
 f_{E1} \propto & (\boldsymbol{\epsilon}' \cdot \boldsymbol{\epsilon}) \alpha_{E1}^{(0)}(\omega) \sum_{n=1}^N e^{-i\mathbf{G}_m \cdot \mathbf{r}_n} \\
 & - i\alpha_{E1}^{(1)}(\omega) (\boldsymbol{\epsilon}' \times \boldsymbol{\epsilon}) \cdot \left[\sum_{n=1}^N e^{-i\mathbf{G}_m \cdot \mathbf{r}_n} \langle \theta_n | \hat{\mathbf{J}} | \theta_n \rangle \right] \\
 & + \alpha_{E1}^{(2)}(\omega) \sum_{\nu=1}^5 P_{\nu}^{(2)}(\boldsymbol{\epsilon}', \boldsymbol{\epsilon}) \left[\sum_{n=1}^N e^{-i\mathbf{G}_m \cdot \mathbf{r}_n} \langle \theta_n | \hat{z}_{\nu} | \theta_n \rangle \right],
 \end{aligned} \tag{5.1}$$

where the wavevector of the m -th satellite spot is defined by

$$\mathbf{G}_m = (0, 0, \tau_m), \quad \tau_m = m \frac{2}{N} \tag{5.2}$$

which is measured in units of $\frac{2\pi}{c}$. The position vector of the n -th Ho layer is represented as $\mathbf{r}_n = (0, 0, \frac{c}{2}n)$.

Now we describe θ_n in various magnetic ordered phase. In the conical phase, it is given by

$$\theta_n = \begin{cases} 2\pi \frac{n}{N} + \phi_0 - \gamma & \text{for } n = \text{odd} \\ 2\pi \frac{n-1}{N} + \phi_0 + \gamma & \text{for } n = \text{even} \end{cases}, \tag{5.3}$$

where ϕ_0 is a constant and taken to be zero. The number of the holmium layers within a helical pitch is $N = 12$. In the uniform helical phase, we could put N as an arbitrary integer, ϕ_0 as an arbitrary angle, and $\gamma = \frac{\pi}{N}$ in eq. (5.3). Thereby we have θ_n for an arbitrary integer n ,

$$\theta_n = \pi \frac{2n-1}{N} + \phi_0. \tag{5.4}$$

In the spin slip phase, we take a case of $N = 11$ system as an example, since the distribution of θ_n 's show a wide diversity. The unit cell consists of the five pairs of bunched doublet

and a single layer as schematically shown in Fig. 1 (c). Within the one helical pitch (for $n = 1, 2, \dots, N$), θ_n 's are expressed as

$$\theta_n = \begin{cases} 2\pi \frac{n}{N+1} + \phi_0 - \gamma & \text{for } n = 1, 3, \dots, N-2 \\ 2\pi \frac{n-1}{N+1} + \phi_0 + \gamma & \text{for } n = 2, 4, \dots, N-1 \\ \frac{2\pi}{N+1} & \text{for } n = N \end{cases}, \quad (5.5)$$

with $\phi_0 = \frac{\pi}{2}$. Note that eq. (5.5) is valid only for $n = 1, \dots, N$, which is enough for the present analysis.

With the use of eqs. (4.1) and (4.2) together with eqs. (5.3), (5.4), and (5.5), the calculation of eq. (5.1) results in evaluating the summations of the types

$$\begin{aligned} & \sum_{n=1}^N e^{-i\mathbf{G}_m \cdot \mathbf{r}_n} \times \begin{Bmatrix} \cos(m'\theta_n) \\ \sin(m'\theta_n) \end{Bmatrix} \\ &= \frac{N}{2} e^{im(\phi_0 - \frac{\pi}{N})} \sum_{\ell} \cos \left[\left(m - \frac{\ell N}{2} \right) \gamma - \frac{m\pi}{N} \right] \\ & \times e^{i\frac{\ell N}{2}(\frac{2\pi}{N} - \phi_0)} \left[\delta_{m+m', \frac{\ell N}{2}} \begin{Bmatrix} 1 \\ i \end{Bmatrix} + \delta_{m-m', \frac{\ell N}{2}} \begin{Bmatrix} 1 \\ (-i) \end{Bmatrix} \right], \end{aligned} \quad (5.6)$$

where ℓ is an arbitrary integer. Note that eq. (5.6) has no contribution when ℓ is a odd integer in the uniform helical phase, since the cosine factor becomes $\cos(\frac{\ell\pi}{2})$ with $\gamma = \frac{\pi}{N}$. In the case of the conical phase, eq. (5.6) is applicable for $m' \geq 1$ and when $m' = 0$, the summation is trivial as $\sum_{n=1}^N e^{-i\mathbf{G}_m \cdot \mathbf{r}_n} = N\delta_{m,0}$.

5.1 Uniform helical phase

In the uniform helical phase, the observed value of N is larger than about seven. Then, only the term proportional to $\delta_{m-m', \frac{\ell N}{2}}$ with $\ell = 0$ in eq. (5.6) is relevant for the description of the $E1$ process in this phase. Practically, eq. (5.6) is rewritten as

$$\begin{aligned} & \sum_{n=1}^N e^{-i\mathbf{G}_m \cdot \mathbf{r}_n} \times \begin{Bmatrix} \cos(m'\theta_n) \\ \sin(m'\theta_n) \end{Bmatrix} \\ & \rightarrow \delta_{m,m'} \frac{N}{2} e^{im(\phi_0 - \frac{\pi}{N})} \cos \left[m \left(\gamma - \frac{\pi}{N} \right) \right] \begin{Bmatrix} 1 \\ (-i) \end{Bmatrix}. \end{aligned} \quad (5.7)$$

By substituting eq. (5.7) into eq. (5.1), and fixing $\beta = \gamma = \frac{\pi}{2}$, we obtain the RXS amplitude at the first satellite spot as

$$f_{E1} \propto -i \frac{N}{2} e^{i(\phi_0 - \frac{\pi}{N})} J[(\boldsymbol{\epsilon}' \times \boldsymbol{\epsilon})_x - i(\boldsymbol{\epsilon}' \times \boldsymbol{\epsilon})_y] \alpha_{E1}^{(1)}(\omega). \quad (5.8)$$

Note that the contributions from the quadrupole operator disappear in the uniform helical phase at the first satellite spot. Similarly, the amplitude at the second satellite spot is given

by,

$$f_{E1} \propto \frac{N}{2} \frac{\sqrt{3}J(2J-1)}{4} e^{2i(\phi_0 - \frac{\pi}{N})} [P_1^{(2)} - iP_5^{(2)}] \alpha_{E1}^{(2)}(\omega), \quad (5.9)$$

where arguments are omitted in the geometrical factor $P_\lambda^{(\nu)}$. As already known,^{10,11,23} the spectrum at the m -th satellite spot consists of pure rank m profile. The final forms of the scattering intensities are derived by substituting the geometrical factors into eqs. (5.8) and (5.9). We relegate both the detail of the derivation and the results to Appendix . Here, we mention an important feature the results possess that the intensities exhibit no ψ dependence at both satellite spots with the choice of the scattering vector as the form in eq. (5.2).

5.2 Conical phase

In the conical phase, N and ϕ_0 are fixed to be twelve and zero, respectively. A notable difference compared with the uniform helical phase is that the terms with $\ell = \pm 1$ becomes to be relevant in eq. (5.6) in the conical phase. Let us state the result with $\ell = 0$ and ± 1 , in turn.

First, the relevant terms in eq. (5.6) with $\ell = 0$ are summarized as follows. At the first satellite spot ($m = 1$), the amplitude is written as

$$\begin{aligned} f_{E1} &\propto 6e^{-i\frac{\pi}{12}} \cos\left(\gamma - \frac{\pi}{12}\right) J \sin \beta \\ &\times \left[-i\{(\epsilon' \times \epsilon)_x - i(\epsilon' \times \epsilon)_y\} \alpha_{E1}^{(1)}(\omega) \right. \\ &\left. + \frac{\sqrt{3}(2J-1) \cos \beta}{2} \{P_4^{(2)} - iP_3^{(2)}\} \alpha_{E1}^{(2)}(\omega) \right]. \end{aligned} \quad (5.10)$$

The amplitude is a mixture of $\alpha_{E1}^{(1)}(\omega)$ and $\alpha_{E1}^{(2)}(\omega)$, while the one is pure $\alpha_{E1}^{(1)}(\omega)$ in the uniform helical phase. This indicates that there is a possibility to observe the variation of the spectral shape of the first satellite spot when the underlying magnetic structure changes. However, such a possibility is practically denied since $|\alpha_{E1}^{(1)}(\omega)|$ is much larger than $|\alpha_{E1}^{(2)}(\omega)|$ as is confirmed numerically in the next section.

The amplitude at the second satellite spot ($m = 2$) is given by,

$$\begin{aligned} f_{E1} &\propto 6e^{-i\frac{\pi}{6}} \cos\left(2\gamma - \frac{\pi}{6}\right) \sin^2 \beta \\ &\times \frac{\sqrt{3}}{4} J(2J-1) [P_1^{(2)} - iP_5^{(2)}] \alpha_{E1}^{(2)}(\omega). \end{aligned} \quad (5.11)$$

Note that both amplitudes do not include a contribution from $\langle \theta_n | \hat{J}_z | \theta_n \rangle$ despite the fact that the conical phase is characterized by the non-zero value of it.

Next, we proceed to summarize the result expected from the terms with $\ell = \pm 1$ in eq. (5.6). This raises a possibility that signals from the higher-order satellites may be detected. The possibility is linked to the distortion of the direction of the magnetic moment within the basal plane. Koehler *et al.* have reported that such higher-order magnetic satellites as fifth- and seventh-order spots were present in the neutron scattering.¹ In the $E1$ process of

R(M)XS, we see the possibility that the intensities from the fourth-, eighth-order in addition to fifth- and seventh-order satellites are detectable. The possibility of detecting the former two satellite enable RXS to be a complement to neutron scattering.

The fifth and seventh satellite spots have contributions from rank one and two profiles. The intensities are proportional to

$$\begin{aligned} \propto & \cos^2 \left(\gamma + \frac{5\pi}{12} \right) \left| -i\{(\boldsymbol{\epsilon}' \times \boldsymbol{\epsilon})_x \pm i(\boldsymbol{\epsilon}' \times \boldsymbol{\epsilon})_y\} \alpha_{\text{E1}}^{(1)}(\omega) \right. \\ & \left. + \frac{\sqrt{3}(2J-1)\cos\beta}{2} \{P_4^{(2)} \pm iP_3^{(2)}\} \alpha_{\text{E1}}^{(2)}(\omega) \right|^2, \end{aligned} \quad (5.12)$$

where $m = \pm 5$ and ± 7 . The upper and lower signs in the equation are taken in accordance with that of m . The intensities at the fourth and eighth satellite spots have contribution from rank two profile, being proportional to

$$\propto \cos^2 \left(2\gamma + \frac{\pi}{3} \right) |P_1^{(2)} \pm iP_5^{(2)}|^2 |\alpha_{\text{E1}}^{(2)}(\omega)|^2, \quad (5.13)$$

where $m = \pm 4$ and ± 8 . The upper and lower signs in the equation are taken in accordance with that of m . The detectabilities of these intensities at the higher order satellite spots are determined by the cosine factors and the geometrical factors appeared in the above expressions. If we assume $\gamma = 5.8^\circ$, the former factor gives 0.08, 0.19, 0.48, and 0.64 with $m = \pm 4, \pm 5, \pm 7$, and ± 8 , respectively. Near Ho M_5 edge, the Bragg angle $\theta^{(m)} = 33.1^\circ, 43.1^\circ$, and 73.0° with respect to $m = \pm 4, \pm 5$, and ± 7 , respectively. With the substitution of these parameter values, we can conclude that the intensity from the $\alpha_{\text{E1}}^{(2)}(\omega)$ contribution at the Ho M_5 fourth satellite spot in the $\pi - \sigma'$ (or $\sigma - \pi'$) channel is large enough to be detected. Actually, the intensity is expected as nearly the same as that observed at the second satellite spot by Ott *et al.*³⁸ Finally, we end this subsection with a comment that the intensities present no azimuthal angle dependence with the choice of \mathbf{G}_m as eq. (5.2) in the conical phase as shown in App. .

5.3 Spin slip phase

Since the magnetic structure of this phase is filled with variation, we restrict ourself on the case of $N = 11$ system depicted in Fig. 1 (c). The distribution of θ_n 's is irregular at the spin-slipped layer in this phase. Then, the summation over n similar to the left hand side of eq. (5.6) is not results in the right hand side of it. As a consequence, there remains the terms for $m \neq m'$. Two prominent properties are readily anticipated. First, the intensities at the first and second satellite spots exhibit ψ dependence. Second, the profiles consist of the mixture of $\alpha_{\text{E1}}^{(1)}(\omega)$ and $\alpha_{\text{E1}}^{(2)}(\omega)$ at both spots, which leads to the situation that both spectra are dominated by $\alpha_{\text{E1}}^{(1)}(\omega)$. The latter point at the first satellite spot is equivalent to the situation observed in the conical phase, eq. (5.10). It brings about no practical change of the spectral shape since $\alpha_{\text{E1}}^{(1)}(\omega)$ always dominates the entire spectrum. On the other hand, the RXS amplitude at the second satellite spot is completely new one, since those in the conical and uniform helical phases are made of pure $\alpha_{\text{E1}}^{(2)}(\omega)$.

5.4 Clockwise or anti-clockwise

In the helical (or conical) magnetic structure of holmium sample, usually, there exist two domains distinguished by the orientation of the winding of the magnetic moment as clockwise and anti-clockwise. The latter is defined such that the angle θ_n of the moment increases anti-clockwise when the number of Ho layer n increases as shown in Fig. 1, while the former the opposite. Since experimentally observed RXS intensities are expected to be the domain averaged quantities, we should mention what is anticipated from the clockwise and anti-clockwise domains.

By checking eqs. (5.8) and (5.9), it turns out that the RXS intensity shows no domain dependence in the uniform helical phase. The same is true at the second satellite spot in the conical phase. The intensity at the first satellite spot, however, shows domain dependence when the scattering vector is not the $(0, 0, \tau_1)$ -type. For example, the intensities with $\mathbf{G} = (2, 1, \tau_1)$ may give domain dependence. Fortunately, such \mathbf{G} is impossible to achieve at the Ho M_5 absorption edge. When the experiment is possible for this scattering vector at the L_3 edge, the domain consideration will be necessary interpreting the result. As a result, it is no need to worry about the domain consideration when analyzing the conical and the uniform helical phases. As for the spin slip phase, the spectrum shows the domain dependence, at least in a qualitative sense, regardless of the scattering vector. So we take domain average when numerical evaluation is carried out in the spin slip phase in the next section.

6. Numerical results

We are now in a position to calculate the RXS spectra in order to compare with the experimental result. Before the comparing process goes forward, we first expect that the sample used in the measurement is in the uniform helical phase, not in the conical nor spin slip phases, because Ott *et al.* explicitly did not reported such information nor temperature the measurement were performed.^{38,41} The data were obtained from the Ho-metal thin film with 16 mono-layers (ML). The critical temperature T_N of the 16 ML sample is about eighty percent of the bulk one³² and the first harmonics satellite peak is observed around $\tau_1 \simeq 0.3 \text{ \AA}^{-1}$.³⁸ This value of τ_1 suggests that the temperature is $T = 0.55T_N$ inferred from Fig. 4 of ref. 38. In bulk Ho, the ratio $T/T_N = 0.55$ corresponds to $T \simeq 73 \text{ K}$ and $\tau_1 = 0.252 \text{ \AA}^{-1}$ with $N \simeq 9$. On the other hand, if we apply the value of τ_1 to the bulk leading to $T \simeq 115 \text{ K}$ with $N \simeq 7.5$.⁷ Since the uniform helical phase is transformed into the spin slip phase below about 50 K with $\tau_1 \simeq 0.22 \text{ \AA}^{-1}$ in the bulk, both estimations lead us to a conclusion that the experiment were performed in the uniform helical phase of the sample as anticipated. Later, we will lend a further support that this assumption is sustained when we calculate the second harmonics satellite spectrum. We show if the sample was in the spin slip phase, the spectral shape might be completely different one. In the following, we assume $N = 8$, i.e., four unit cells are involved in one helical pitch. We emphasize that the choice of N does not alter the

spectral shapes.

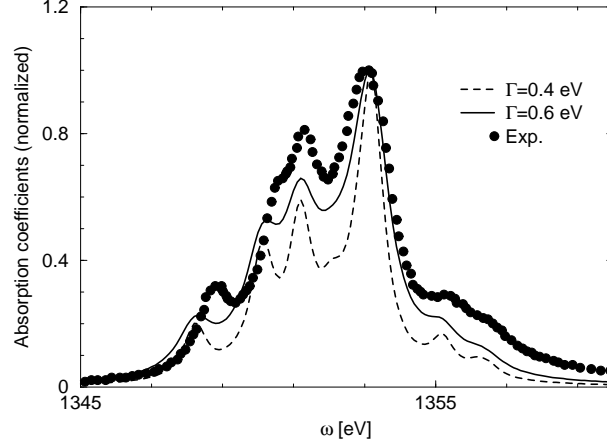


Fig. 2. Absorption coefficient at the Ho M_5 edge corresponding to $-\text{Im}\alpha_{E1}^{(0)}(\omega)$. The solid and dashed lines are obtained with $\Gamma = 0.6$ and 0.4 eV, respectively. Filled circles are the experimental data.³⁸

6.1 Absorption coefficients

We discuss the absorption coefficient $A(\omega)$ in the $E1$ transition, which is described as

$$A(\omega) \propto \Gamma \sum_j \sum_{\Lambda} \sum_{\alpha} \frac{|\langle \Lambda | x_{j,\alpha}(j) | \psi_0 \rangle|^2}{(\hbar\omega - E_{\Lambda})^2 + \Gamma^2}. \quad (6.1)$$

It is obtained from eq. (3.3) by the relation

$$A(\omega) \propto -\text{Im}\alpha_{E1}^{(0)}(\omega), \quad (6.2)$$

where $\text{Im}X$ represents the imaginary part of X . Although the absorption spectrum at the Ho M_5 edge was already investigated by others,^{6,15} here, we utilize it in three-fold purposes; the determination of the origin of the energy, that of the value of Γ , and the justification of the atomic picture.

The calculated result is shown in Fig. 2. The origin of the energy is adjusted such that the maximum point is located at the experimental one, i.e., at 1353.2 eV and is fixed throughout this paper. Since the peak structure of the spectrum shows Γ dependence, several values of Γ are examined. As shown in Fig. 2, we find $\Gamma \sim 0.6$ eV gives a better choice. We do not try, however, to obtain the best fit to the data considering the simple treatment based on the atomic picture.

This value of Γ is consistent with the previous work for the absorption spectra.⁶ We confirm that the small change of the Γ value around 0.6 eV has no effect on the peak positions. Our result reproduces the characteristic multi-peak structure exhibited by the experimental data.³⁸ The total width of the spectrum is governed by the multiplet splitting of the energy of the intermediate states. Aside from the peak position around 1348.5 eV in the experiment, we

conclude that the atomic treatment gives a reasonable result. Fortunately, we shall confirm in the next subsection that this discrepancy causes no practical effect on the investigation of the RXS spectra, since the intensities near 1348.5 eV at the first and second satellite spots are weak and merely the tail part of the spectra.

6.2 First and second harmonics satellite

The RXS spectral intensities at the first and second harmonics satellite spots are proportional to the dipole ($|\alpha_{\text{E1}}^{(1)}|^2$) and the quadrupole ($|\alpha_{\text{E1}}^{(2)}|^2$) profiles, respectively. The analytical forms are derived by substituting $\beta = \frac{\pi}{2}$ and $\gamma = \frac{\pi}{N}$ into eqs. (A.4) and (A.5) as shown below. The intensity at the first satellite spot is proportional to

$$I^{(1)} \propto \left(J \cos \theta^{(1)} \right)^2 |\alpha_{\text{E1}}^{(1)}(\omega)|^2 \begin{cases} 0 & \text{for } \sigma - \sigma' \\ 1 & \text{for } \sigma - \pi' \\ 1 & \text{for } \pi - \sigma' \\ 4 \sin^2 \theta^{(1)} & \text{for } \pi - \pi' \end{cases}, \quad (6.3)$$

and the one at the second satellite spot is proportional to

$$I^{(2)} \propto \left[\frac{3J(2J-1)}{8} \right]^2 |\alpha_{\text{E1}}^{(2)}(\omega)|^2 \begin{cases} 1 & \text{for } \sigma - \sigma' \\ \sin^2 \theta^{(2)} & \text{for } \sigma - \pi' \\ \sin^2 \theta^{(2)} & \text{for } \pi - \sigma' \\ \sin^4 \theta^{(2)} & \text{for } \pi - \pi' \end{cases}. \quad (6.4)$$

As seen from the above expressions, the RXS intensities show no ψ dependence. Note that spectral shapes have no polarization dependence. In order to compare our results with the experimental ones, we consider the spectra in the $\pi - \sigma'$ and $\pi - \pi'$ channels. The ratio $I^{(1)}/I^{(2)}$ is common in both channels with an aid of the relation $\sin \theta^{(2)} = 2 \sin \theta^{(1)}$. Thus, we can fix $\psi = 0$ and restrict in the $\pi - \sigma'$ channel hereafter. The calculated spectra of $I^{(1)}$ and $I^{(2)}$ are shown in the upper and lower panels, respectively, of Fig. 3 together with the experimental data.⁴²

As for the $|\alpha_{\text{E1}}^{(1)}|^2$ from the first satellite spot with $\mathbf{G}_1 = (0, 0, \tau_1)$, the peak position of the spectrum appears at the same position of the absorption coefficient, which is coincide with the experiment. The entire spectral shape with $\Gamma = 0.6$ eV agrees remarkably well with the experimental one including the kink in the low energy tail and the hump in the high energy tail.

As for the $|\alpha_{\text{E1}}^{(2)}|^2$ from the second satellite spot with $\mathbf{G}_2 = (0, 0, \tau_2)$, the maximum height intensity is located at the energy 1.8 eV lower than that of the absorption as the same position as the experiment. The entire spectral width and the shape of the tail parts show quite similar to the experiment, too. On the other hand, however, a prominent discrepancy can be found between the theory and the experiment. The peak around 1353 eV found in the the calculated result is absent in the experiment. The reason of this discrepancy is still unclear. From the

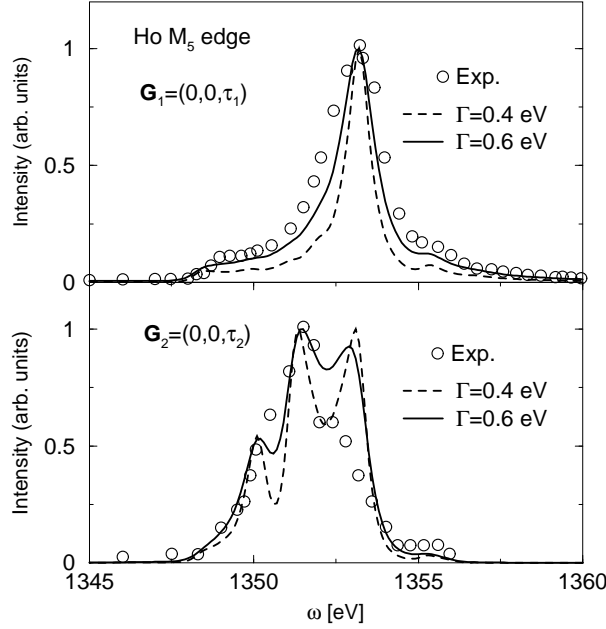


Fig. 3. The RXS spectra near the Ho M_5 edge at the first (upper) and second (lower) satellite spots. The curves for $\Gamma = 0.4$ eV and 0.6 eV are distinguished by the dashed and solid lines, respectively. Open circles represent the experimental result.³⁸

calculated value of the ratio $I^{(1)}/I^{(2)}$, we deduce a ratio

$$\frac{|\alpha_{E1}^{(1)}(\omega)|}{|\alpha_{E1}^{(2)}(\omega)|} \simeq 27.7, \quad (6.5)$$

with $\Gamma = 0.6$ eV. This large ratio allows us to expect the dominance of $\alpha_{E1}^{(1)}(\omega)$ in the entire spectral shape when both profiles are mixed.

6.3 M_4 edge

We carry out the similar calculations at the Ho M_4 edge as those at the M_5 edge. The absorption coefficient is shown in the upper panel of Fig. 4. It shows a single peak structure and the peak height of the M_4 spectrum is about 0.175 times the one at the M_5 edge. These observations agree with the experiment.⁶ The RXS spectra expected from the first and second harmonics satellite spots are shown in the lower panel of Fig. 4. The maximum intensity of the second satellite spectrum is found at the energy about 0.6 eV higher than that of the first satellite spectrum. This tendency is contrary to the case observed at the M_5 edge where the former is found at the energy about 1.8 eV lower than the latter. The peak intensities at the M_4 edge are about two times weaker than those at the M_5 edge. Since the order of the magnitude of the spectrum of the first satellite spot at the M_4 edge is roughly the same order as that of the second satellite spot at the M_5 spot, the former may be detectable experimentally.

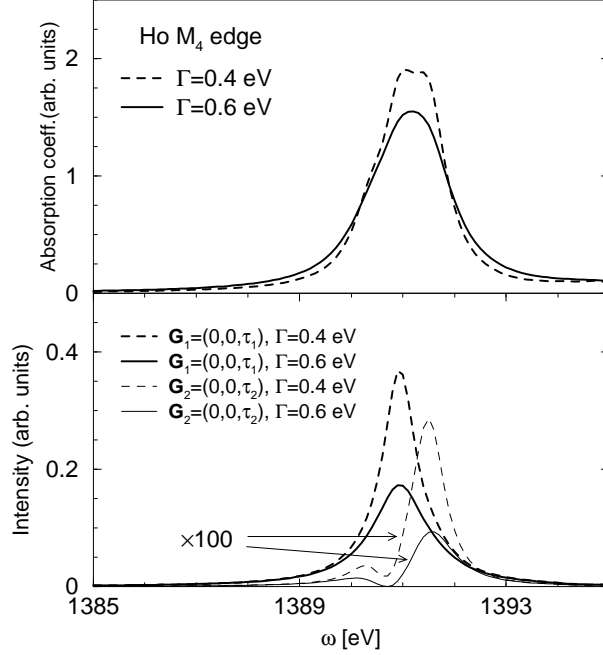


Fig. 4. Absorption coefficient and the RXS spectra at the Ho M_4 edge. Upper: the absorption coefficients with $\Gamma = 0.6$ eV and 0.4 eV are shown by the solid and dashed lines, respectively. Lower: the RXS spectra at the first and second harmonics satellite spots are represented by the thick and thin lines, respectively. The values of $\Gamma = 0.4$ eV and 0.6 eV are distinguished by the dashed and solid lines, respectively.

6.4 *spin-slip phase*

We investigate the RXS spectra at the satellite spot in the spin slip phase. The qualitative evaluation in Sec. 5.3 indicates that they are the mixture of the profiles $\alpha_{E1}^{(1)}(\omega)$ and $\alpha_{E1}^{(2)}(\omega)$. The dominance of the former over the latter leads to the expectation that the spectra at the first and second satellite spots in this phase are governed by the former. The situation at the second satellite spot is of particular interest since the spectra consist of the pure $\alpha_{E1}^{(2)}(\omega)$ both in the conical and the uniform helical phases. Quantitatively, we calculate the RXS spectrum at the second satellite spot in a spin slip phase with $N = 11$. The core hole lifetime broadening is set to be 0.6 eV. As shown in Sec. 5.4, the spectra exhibit the domain dependence, that is, the clockwise or anti-clockwise alternation of the direction of the magnetic moment affect the spectra. Thus we take the domain average of the spectra assuming equal probability of the two domain. Moreover, the spectrum varies as a function of ψ in this phase. The results are summarize in Fig. 5. Although the spectral shape varies with ψ , the entire shape including the highest peak position is dominated by the pure $|\alpha_{E1}^{(1)}(\omega)|^2$ as anticipated qualitatively.

This fact brings us to the speculation of the spectral shape evolution. With decreasing temperature from T_N down to T_C , the spectral shape at the second satellite spot evolves from

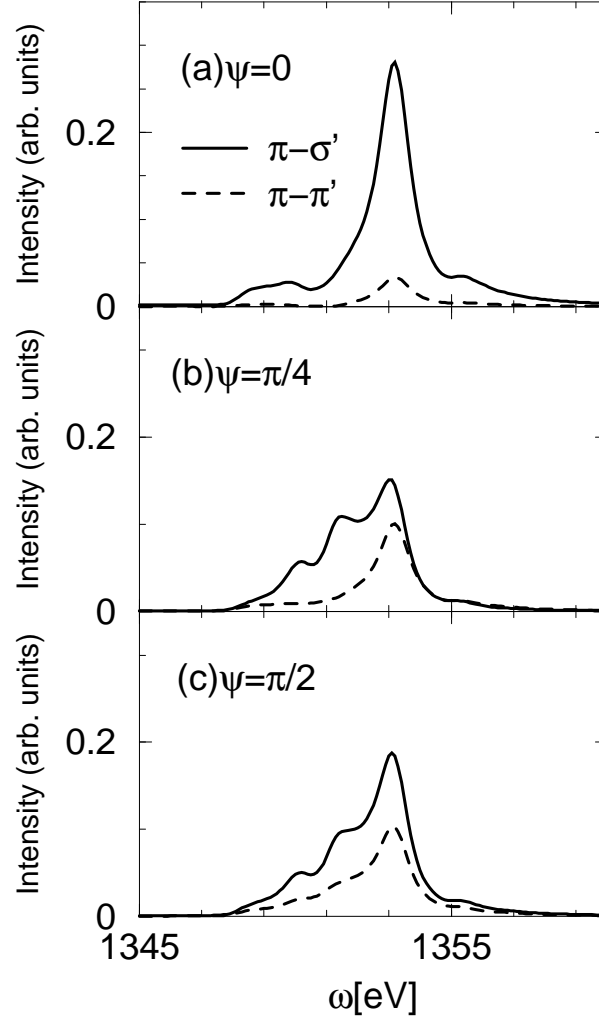


Fig. 5. The RXS spectra at the Ho M_5 edge with $\mathbf{G}_2 = (0, 0, \tau_2)$ in the spin slip phase with $N = 11$.

The intensities are averaged between the anti-clockwise and clockwise helical phases. The solid and broken lines represent the $\pi - \sigma'$ and $\pi - \pi'$ channels, respectively. The azimuthal angles are chosen as (a) $\psi = 0$, (b) $\psi = \frac{\pi}{4}$, and (c) $\psi = \frac{\pi}{2}$.

the pure $|\alpha_{\text{E1}}^{(2)}(\omega)|^2$, through the $|\alpha_{\text{E1}}^{(1)}(\omega)|^2$ dominated one, into the original one accompanying the shift of peak position from 1353.2 eV to 1351.4 eV and again to 1353.2 eV, respectively, large enough to detect experimentally. An experimental observation of the second satellite spot spectra in the different phases is desirable.

7. Concluding remarks

Stimulated by the RMXS experiments,^{34,38} we have investigated the Ho M_5 spectra at the first and second satellite spots. The analysis have performed by exploiting the useful expression of the scattering amplitude derived on the basis of the localized electron picture.^{35,37} Although a large enhancement of the intensity is expected at the Ho M edge in the RXS spectrum, the

spectrum shows no azimuthal angle dependence in the uniform helical and conical phases with the choice of \mathbf{G}_m adopted in the experiment. Thus, we have mainly focused on the spectral shape analysis.

A qualitative analysis have revealed that the RXS spectrum at the first satellite spot consists of the pure rank one energy profile ($\alpha_{E1}^{(1)}(\omega)$) in the uniform helical phase. Upon cooling temperature, the spectrum comprises that of the rank two ($\alpha_{E1}^{(2)}(\omega)$) as well as $\alpha_{E1}^{(1)}(\omega)$ both in the spin slip and conical phases. On the other hand, the spectrum at the second satellite spot is made up of the pure $\alpha_{E1}^{(2)}(\omega)$ in the uniform helical and conical phases. In the spin slip phase, however, the spectrum includes $\alpha_{E1}^{(1)}(\omega)$ too. Our numerical calculation have revealed that the magnitude of the $|\alpha_{E1}^{(1)}(\omega)|$ is much larger than $|\alpha_{E1}^{(2)}(\omega)|$, for instance, $|\alpha_{E1}^{(1)}(\omega)|/|\alpha_{E1}^{(2)}(\omega)| \simeq 27.7$ with $\Gamma = 0.6$ eV. Thus, whenever both profiles mix, we can expect the $\alpha_{E1}^{(1)}(\omega)$ dominates the spectral shape. Then, the spectrum at the first satellite spot looks like $|\alpha_{E1}^{(1)}(\omega)|^2$ at all magnetic phases. Contrary to this, we conclude that the spectral shape of the second satellite spot varies as a function of temperature. That is, the spectrum is pure $|\alpha_{E1}^{(2)}(\omega)|^2$ in the helical phase, then looks like $|\alpha_{E1}^{(1)}(\omega)|^2$ in the spin slip phase, and finally, becomes pure $|\alpha_{E1}^{(2)}(\omega)|^2$ again in the conical phase. If such variation of the spectral shape would be observed by the experiment, it demonstrates a clear evidence of the change of the magnetic structures.

If the experiment in the conical phase is attainable, another attractive outcome can be expected. That is, the RXS spectrum from the higher-order harmonic satellite spots may be detected. It is brought about by the distortion of the orientation of the magnetic moment within the basal plane. In neutron scattering, the signals at the (6 ± 1) th magnetic satellite spots were observed.¹ In the present case of RXS in the $E1$ transition, the intensities at the (6 ± 2) th as well as (6 ± 1) th order satellite spots, which are related to rank two and one operators, respectively, will be detected. By evaluating the Ho case in the vicinity of the M_5 absorption edge, we can conclude that the intensity at the fourth satellite spot is within the reach of the present experimental condition of the $E1$ transition in the $\pi - \sigma'$ channel.

As for the numerical results, first, we have concentrated on the comparison of our result with the experiment in the uniform helical phase. The calculated RXS spectrum at the first satellite spot and the absorption coefficient show excellent agreement with the observed ones both the spectral shape and the peak position (for the former spectrum).^{6,15,38} The agreement assures the reliability of the present analysis based on the localized picture. At the same time, it also demonstrates the effectiveness of the spectral shape analysis in the RXS theory, which is rare, in particular, in the f -electron systems. The agreement of the spectrum at the second satellite spot between ours and the experiment is not an ideal one. Although the peak position, below about 1.8 eV compared to that of the first satellite spectrum, is properly reproduced, the theory includes an extra peak around 1353.2 eV which is missing in the experiment. The

reason of this discrepancy is still unclear.

Next, our evaluation of the spectra at the M_4 edge showed that the magnitudes of them are roughly two orders of magnitude smaller than those at the M_5 edge. Thus, the possibility of experimental detection seems to be slim at the second satellite spot. On the other hand, the magnitude of the spectrum at the first satellite spot at the M_4 is expected to be the same order as that of the second satellite spot at the M_5 edge, and seems to be detectable. Finally, we have confirmed that the spectrum the second satellite spot in the spin slip phase certainly governed by the $|\alpha_{E1}^{(1)}(\omega)|$ as anticipated.

A qualitative part of the present analysis may be applicable to the interpretation of the RMXS experiment near the Ho L_3 edge in the $E1$ process, by neglecting the band nature of the $5d$ electrons as the previous works had followed.^{10,11,13} Since the absorption coefficient at the L_3 edge exhibited no multi-peak structure, we conclude either the multiplet splitting of the intermediate are not large enough and/or the energy resolution were not fine enough to distinguish the line shapes of the different profiles $\alpha_{E1}^{(1)}(\omega)$ and $\alpha_{E1}^{(2)}(\omega)$. Thus, only we can guess is the polarization analysis. If the sample used were in the uniform helical phase, eqs. (6.3) and (6.4) state that the spectra at the first and second satellite spots are pure $\alpha_{E1}^{(1)}(\omega)$ and $\alpha_{E1}^{(2)}(\omega)$, respectively. The former is absent in the $\sigma - \sigma'$ channel. The latter has contributions both in the $\sigma - \sigma'$ and $\sigma - \pi'$ channels. These conclusions are just the ones deduced previously.^{10,11,13,23} Note that, in ref. 13, although the authors concluded there was no $E1$ contribution in the $\sigma - \pi'$ channel at the second satellite spot $(0, 0, 2 + 2\tau)$, the data exhibits a small hump around 8071 eV, at which the $E1$ peak is expected. By substituting the value of the Bragg angle ($\theta^{(2)} \simeq 18^\circ$) in eq. (6.4), the intensity of the $\sigma - \pi'$ channel in the $E1$ process is evaluated about a tenth of that in the $\sigma - \sigma'$ channel. Since the ratio is nearly equal to that observed, the data may show the contribution from the $E1$ process in the $\sigma - \pi'$ channel at the second satellite spot. Thus the intensity around this energy may show the resonant behavior. Additionally, the analysis on the $E2$ process by means of the present theory qualitatively shows complete agreement with the previous interpretation.^{10,11,23} Because our formalism allows naturally inclusion of the energy profile analysis, such an investigation is the next step along this line.⁴³

Since the wavelength of soft x-ray is suitable for the investigation of the long periodic magnetic structure observed in several heavy rare earth material, the present theory may be effective for the analysis of the R(M)XS spectra at the $M_{4,5}$ edges of such heavy rare earth compounds, for example, DyB_2C_2 . Actually, the absorption coefficient in the vicinity of the Dy M_5 edge exhibits multi-peak structure similar to that observed in Ho.^{6,39} On the other hand, the RXS spectra differ significantly between those of Dy and Ho. The spectrum of Dy extends over a few tens eV, an order of magnitude wider than that of Ho, which may not be explained within the present localized electron picture.³⁹ The work along this line is a future

study.

Acknowledgments

We thank M. Takahashi for valuable discussions. This work was partially supported by a Grant-in-Aid for Scientific Research from the Ministry of Education, Science, Sports and Culture, Japan.

Appendix: The geometrical factors and the scattering amplitude

Here, we present the geometrical factors needed to evaluate eqs. (5.10) and (5.11). The results are classified by the photon polarizations. The origin of ψ is defined such that the y axis lies in the scattering plane. The geometrical configuration we adopted in this work can be found in our previous paper.³⁷ For the first satellite spot $\mathbf{G}_1 = (0, 0, \tau_1)$,

$$(\boldsymbol{\epsilon}' \times \boldsymbol{\epsilon})_x - i(\boldsymbol{\epsilon}' \times \boldsymbol{\epsilon})_y = e^{i\psi} \cos \theta^{(1)} \begin{cases} 0 & \text{for } \sigma - \sigma' \\ -i & \text{for } \sigma - \pi' \\ i & \text{for } \pi - \sigma' \\ -2 \sin \theta^{(1)} & \text{for } \pi - \pi' \end{cases}, \quad (\text{A}\cdot 1)$$

and

$$P_4^{(2)}(\boldsymbol{\epsilon}', \boldsymbol{\epsilon}) - iP_3^{(2)}(\boldsymbol{\epsilon}', \boldsymbol{\epsilon}) = \frac{\sqrt{3}}{2} e^{i\psi} \cos \theta^{(1)} \begin{cases} 0 & \text{for } \sigma - \sigma' \\ 1 & \text{for } \sigma - \pi' \\ 1 & \text{for } \pi - \sigma' \\ 0 & \text{for } \pi - \pi' \end{cases}, \quad (\text{A}\cdot 2)$$

where $\theta^{(1)}$ is the Bragg angle associated with \mathbf{G}_1 . Then, for the second satellite spot \mathbf{G}_2 ,

$$P_1^{(2)}(\boldsymbol{\epsilon}', \boldsymbol{\epsilon}) - iP_5^{(2)}(\boldsymbol{\epsilon}', \boldsymbol{\epsilon}) = \frac{\sqrt{3}}{2} e^{2i\psi} \begin{cases} 1 & \text{for } \sigma - \sigma' \\ i \sin \theta^{(2)} & \text{for } \sigma - \pi' \\ -i \sin \theta^{(2)} & \text{for } \pi - \sigma' \\ \sin^2 \theta^{(2)} & \text{for } \pi - \pi' \end{cases}, \quad (\text{A}\cdot 3)$$

where $\theta^{(2)}$ is the Bragg angle associated with \mathbf{G}_2 . Note that a relation $\sin \theta^{(2)} = 2 \sin \theta^{(1)}$ holds.

By substituting these results into eqs. (5.10) and (5.11), we obtain the RXS intensities at the first satellite spot as

$$|f_1|^2 \propto \left[\frac{N}{2} \cos \left(\gamma - \frac{\pi}{N} \right) J \sin \beta \cos \theta^{(1)} \right]^2 \times \begin{cases} 0 & \text{for } \sigma - \sigma' \\ \left| \alpha_{\text{E1}}^{(1)}(\omega) + \frac{3(2J-1) \cos \beta}{4} \alpha_{\text{E1}}^{(2)}(\omega) \right|^2 & \text{for } \sigma - \pi' \\ \left| \alpha_{\text{E1}}^{(1)}(\omega) - \frac{3(2J-1) \cos \beta}{4} \alpha_{\text{E1}}^{(2)}(\omega) \right|^2 & \text{for } \pi - \sigma' \\ 4 \sin^2 \theta^{(1)} |\alpha_{\text{E1}}^{(1)}(\omega)|^2 & \text{for } \pi - \pi' \end{cases}, \quad (\text{A}\cdot 4)$$

and the one at the second satellite spot as

$$\begin{aligned}
 |f_1|^2 &\propto \left[\frac{3N}{16} \cos \left(2\gamma - \frac{2\pi}{N} \right) J(2J-1) \sin^2 \beta \right]^2 \\
 &\times |\alpha_{\text{E1}}^{(2)}(\omega)|^2 \begin{cases} 1 & \text{for } \sigma - \sigma' \\ \sin^2 \theta^{(2)} & \text{for } \sigma - \pi' \\ \sin^2 \theta^{(2)} & \text{for } \pi - \sigma' \\ \sin^4 \theta^{(2)} & \text{for } \pi - \pi' \end{cases} . \quad (\text{A}\cdot 5)
 \end{aligned}$$

These results show the spectral intensities exhibit no azimuthal angle dependence.

References

- 1) W. C. Koehler, J. W. Cable, M. K. Wilkinson, and E. O. Wolian: Phys. Rev. **151** (1966) 414.
- 2) W. C. Koehler, J. W. Cable, H. R. Child, M. K. Wilkinson, and E. O. Wolian: Phys. Rev. **158** (1967) 450.
- 3) G. P. Felcher, G. H. Lander, T. Arai, S. K. Sinha, and F. H. Spedding: Phys. Rev. B **13** (1976) 3034.
- 4) R. Cowan: *The Theory of Atomic Structure and Spectra* (University of California Press, Berkeley, 1981).
- 5) M. Blume: J. Appl. Phys. **57** (1985) 3615.
- 6) B. T. Thole, G. van der Laan, J. C. Fuggle, G. A. Sawatzky, R. C. Karnatak, and J. -M. Esteve: Phys. Rev. B **32** (1985) 5107.
- 7) D. Gibbs, D. E. Moncton, K. L. D'Amico, J. Bohr, and B. H. Grier: Phys. Rev. Lett. **55** (1985) 234.
- 8) K. Namikawa, M. Ando, T. Nakajima, and H. Kawata: J. Phys. Soc. Jpn. **54** (1985) 4099.
- 9) M. J. Pechan and C. Stassis: J. Phys. Rev. C **21** (1988) 4113.
- 10) D. Gibbs, D. R. Harshman, E. D. Isaacs, D. B. McWhan, D. Mills, and C. Vettier: Phys. Rev. Lett. **61** (1988) 1241.
- 11) J. P. Hannon, G. T. Trammell, M. Blume, and D. Gibbs: Phys. Rev. Lett. **61** (1988) 1245 [Errata; **62** (1989) 2644].
- 12) D. B. McWhan, C. Vettier, E. D. Isaacs, G. E. Ice, D. P. Siddons, J. B. Hastings, C. Peters, and O. Vogt: Phys. Rev. B **42** (1990) 6007.
- 13) D. Gibbs, G. Grübel, D. R. Harshman, E. D. Isaacs, D. B. McWhan, D. Mills, and C. Vettier: Phys. Rev. B **43** (1991) 5663.
- 14) C. C. Tang, W. G. Stirling, G. H. Lander, D. Gibbs, W. Herzog, P. Carra B. T. Thole, K. Mat-tenberger, and O. Vogt: Phys. Rev. B **46** (1992) 5287.
- 15) J. Ph. Schillé, J. P. Kappler, Ph. Saintavit, Ch. Cartier dit Moulin, C. Brouder, and G. Krill: Phys. Rev. B **48** (1993) 9491.
- 16) T. R. Thurston, G. Helgesen, J. P. Hill, D. Gibbs, B. D. Gaulin, and P. J. Simpson: Phys. Rev. B **49** (1994) 15730.
- 17) G. Helgesen, J. P. Hill, T. R. Thurston, D. Gibbs, J. Kwo, and M. Hong: Phys. Rev. B **50** (1994) 2990.
- 18) P. Carra and B. T. Thole: Rev. Mod. Phys. **66** (1994) 1509.
- 19) M. Blume: in *Resonant anomalous x-ray scattering*, eds. G. Materlik and C. J. Sparks and K. Fischer (North-Holland, Amsterdam, 1994), p. 495.
- 20) J. A. Simpson, D. F. McMorrow, R. A. Cowley, and D. A. Jehan: Phys. Rev. B **51** (1995) 16073.
- 21) S. W. Lovesey and E. Balcar: J. Phys.: Condens. Matter **8** (1996) 10983.
- 22) J. Jensen: Phys. Rev. B **54** (1996) 4021.
- 23) J. P. Hill and D. F. McMorrow: Acta Crystallogr., Sect. A **52** (1996) 236.
- 24) Y. Murakami, H. Kawada, H. Kawata, M. Tanaka, T. Arima, Y. Moritomo, and Y. Tokura: Phys. Rev. Lett. **80** (1998) 1932.
- 25) Y. Tanaka, T. Inami, T. Nakamura, H. Yamauchi, H. Onodera, K. Ohyama, and Y. Yamaguchi: J. Phys.: Condens. Matter **11** (1999) L505.

- 26) K. Hirota, N. Oumi, T. Matsumura, H. Nakao, Y. Wakabayashi, Y. Murakami, and Y. Endoh: Phys. Rev. Lett. **84** (2000) 2706.
- 27) E. N. Ovchinnikova and V. E. Dmitrienko: Acta Crystallogr., Sect. A **56** (2000) 2.
- 28) H. Nakao, K. Magishi, Y. Wakabayashi, Y. Murakami, K. Koyama, K. Hirota, Y. Endoh, and S. Kunii: J. Phys. Soc. Jpn. **70** (2001) 1857.
- 29) F. Yakhov, V. Plakhty, H. Suzuki, S. Gavrilov, P. Burlet, L. Paolasini, C. Vettier, and S. Kunii: Phys. Lett. A **285** (2001) 191.
- 30) See for a review, C. Vettier: J. Electron Spectrosc. Relat. Phenom. **117-118** (2001) 113.
- 31) J. A. Paixão, C. Detlefs, M. J. Longfield, R. Caciuffo, P. Santini, N. Bernfoeft, J. Rebizant, and G. H. Lander: Phys. Rev. Lett. **89** (2002) 187202.
- 32) E. Weschke, H. Ott, E. Schierle, C. Schüßler-Langeheine D. V. Vyalikh, G. Kaindl, V. Leiner, M. Ay, T. Schmitte, and H. Zabel: Phys. Rev. Lett. **93** (2004) 157204.
- 33) D. Mannix, Y. Tanaka, D. Carbone, N. Bernhoeft, and S. Kunii: Phys. Rev. Lett. **95** (2005) 117206.
- 34) P. D. Spencer, S. B. Wilkins, P. D. Hatton, S. D. Brown, T. P. A. Hase, J. A. Purton, and D. Fort: J. Phys.: Condens. Matter **17** (2005) 1725.
- 35) T. Nagao and J. Igarashi: Phys. Rev. B **72** (2005) 174421.
- 36) T. Nagao and J. Igarashi: J. Phys. Soc. Jpn. Suppl. **74** (2005) 247.
- 37) T. Nagao and J. Igarashi: Phys. Rev. B **74** (2006) 104404.
- 38) H. Ott, C. Schüßler-Langeheine, E. Schierle, A. Yu. Grigoriev, V. Leiner, H. Zabel, G. Kaindl, and E. Weschke: Phys. Rev. B **74** (2006) 094412.
- 39) A. M. Mulders, U. Staub, V. Scagnoli, S. W. Lovesey, E. Balcar, T. Nakamura, A. Kikkawa, G. van der Laan, and J. M. Tonnerre: J. Phys.: Condens. Matter **18** (2006) 11195.
- 40) In solids, the magnitude of the Slater integral is reduced because of large screening effect. The isotropic and the anisotropic parts of the Slater integral are reduced their values by multiplying factors 0.25 and 0.8, respectively.
- 41) Data reported in ref. 34 were measured for bulk sample. However, the authors themselves said the precision of the spectral shapes of their data was suspicious. We do not compare our results with them in the present work.
- 42) Since the experimental data in ref. 38 are given as the scattering amplitudes, we plotted them after taking the square of the original data.
- 43) When we discuss the $E2$ process, the geometrical factors appeared in ref. 37 should be replaced by the corrected ones. eqs. (2.18), (2.19), (B1)~(B5), (B7), and (B8) should be multiplied by $3/4$, while eq. (B6) by $\sqrt{3}/4$. The coefficient of $P_\mu^{(1)}$ in eq. (B2) and that of $P_1^{(0)}$ in eq. (B4) should be replaced by $1/2$ and $-\sqrt{5}$, respectively.